Cutaneous Hypervascularization Treatment Using Photo-Mediated Ultrasound Therapy

Mingyang Wang[1,7], Rohit Singh[2,3,4,7], Wei Zhang[1], Jeffrey S. Orringer[5], Yannis M. Paulus[1,6], Xinmai Yang[3,4] and Xueding Wang[1]

Photo-mediated ultrasound therapy (PUT) is a cavitation-based, highly selective antivascular technique. In this study, the effectiveness and safety of PUT on cutaneous vascular malformation was examined through in vivo experiments in a clinically relevant chicken wattle model, whose microanatomy is similar to that of port-wine stain and other hypervascular dermal diseases in humans. Assessed by optical coherence tomography angiography, the blood vessel density in the chicken wattle decreased by 73.23% after one session of PUT treatment in which 0.707 J/cm^2 fluence laser pulses were applied concurrently with ultrasound bursts ($n = 7$, $P < .01$). The effectiveness of removing blood vessels in the skin at depth up to 1 mm was further assessed by H&E-stained histology at multiple time points, which included days 1, 3, 7, 14, and 21 after treatment. Additional immunohistochemical analyses with CD31, caspase-3, and Masson's trichrome stains were performed on day 3 after treatment. The results show that the PUT-induced therapeutic effect was confined and specific to blood vessels only, whereas unwanted collateral damage in other skin tissues such as collagen was avoided. The findings from this study demonstrate that PUT can efficiently and safely remove hypervascular dermal capillaries using laser fluence at a level that is orders of magnitude smaller than that used in conventional laser treatment of vascular lesions, thus offering a safer alternative technique for clinical management of cutaneous vascular malformations.

JID Innovations (2023);**3:**100237 doi:10.1016/j.xjidi.2023.100237

INTRODUCTION

Port-wine stain (PWS) is a congenital skin condition involving abnormal dilation of capillaries and postcapillary venules. It occurs in 0.3% of newborns with a neonatal morbidity rate of 0.3 to 0.5% (Jacobs and Walton, 1976). PWS generally shows progressive growth with the age of the patient and may become hypertrophic and more resistant to treatment (Fu et al, 2019). Children with facial PWS may suffer discrimination from peers, whereas adolescents and adults with PWS can have negative effects on their social life and may suffer from psychological disabilities (Wanitphakdeedecha et al, 2021). Apart from cosmetic and psychological effects, PWS may also impair hearing, speech, sight, and nasal breathing (Eivazi et al, 2012). Therefore, PWS is both a medical and psychological disorder.

In the clinic, laser-based therapies are used for the treatment of PWS (Chen et al, 2012). Currently, pulsed dye laser (PDL) therapy, which is based on the principle of selective photothermolysis, is the most widely used treatment technique for PWS (Morelli et al, 1986). The modern-generation PDL systems using lasers working at 585 and 595 nm, benefiting from the lower optical attenuations of tissue at these longer wavelengths, can be more effective for treating relatively deeper vessels (Asahina et al, 2006; Geronemus et al, 2000; Kono et al, 2007; Tan et al, 1989; Woo et al, 2006). However, PDL is still often ineffective for the treatment of deep small-size vessels, and currently, at least 20 to 30% of PWS are resistant to PDL therapy (Savas et al, 2013).

Apart from PDL, other laser systems such as the Alexandrite laser (755 nm) and Nd:YAG (neodymium-doped yttrium aluminum garnet) laser (1064 nm) are also used for the treatment of PWS. Emitting near-infrared light at 755 nm, the Alexandrite laser has a higher penetration depth in soft tissue and is primarily used for dark or resistant lesions (Izikson and Anderson, 2009; Izikson et al, 2009). The 1064 nm light from the Nd:YAG laser has the highest penetration depth and lowest melanin absorption among all the treatment lasers for PWS. This wavelength has been found to be effective in treating deep and darker PWS (Zhong et al, 2014). However, the 1064 nm can result in adverse side effects such as scarring at higher fluences (van Drooge et al, 2013).

New treatment modalities for PWS are being explored to overcome the limitations of current laser-based therapies (Chen et al, 2012). Photodynamic therapy is a potential

[1]*Department of Biomedical Engineering, University of Michigan, Ann Arbor, Michigan, USA;* [2]*PhotoSonoX LLC, Ann Arbor, Michigan, USA;* [3]*Institute for Bioengineering Research, University of Kansas, Lawrence, Kansas, USA;* [4]*Department of Mechanical Engineering, School of Engineering, University of Kansas, Lawrence, Kansas, USA;* [5]*Department of Dermatology, University of Michigan, Ann Arbor, Michigan, USA; and* [6]*Department of Ophthalmology and Visual Sciences, University of Michigan, Ann Arbor, Michigan, USA*

[7]*These authors contributed equally to this work.*

Correspondence: Xueding Wang, Department of Biomedical Engineering, University of Michigan, 2200 Bonisteel Boulevard, Ann Arbor, Michigan 48109, USA. E-mail: xdwang@umich.edu

Abbreviations: 3D, three-dimensional; FUS, focused ultrasound; MTC, Masson's trichrome; OCT, optical coherence tomography; OCT-A, optical coherence tomography angiography; PDL, pulsed dye laser; PDMS, polydimethylsiloxane; PUT, photo-mediated ultrasound therapy; PWS, port-wine stain

Received 19 January 2023; revised 11 September 2023; accepted 14 September 2023; accepted manuscript published online XXX; corrected proof published online XXX

Cite this article as: JID Innovations 2023;3:100237

alternative for PDL (Orenstein et al, 1990). In photodynamic therapy, a chemical photosensitizer is intravenously injected into the bloodstream, and then the PWS area is irradiated with laser light at a wavelength specific to the photosensitizer. The absorption of light by the photosensitizer creates a photochemical–biological reaction that destroys endothelial cells and shuts down the vasculature (Lu et al, 2010). Studies have found the therapeutic efficiency of photodynamic therapy to be equivalent or superior to that of PDL (Yuan et al, 2008). However, the major drawback of photodynamic therapy for patients is the required photoprotection from direct sunlight for up to 4 weeks (Yuan et al, 2009). During a laser-based treatment, PWS vessels can be shut down, but reperfusion and remodeling of the vasculature often take place after the treatment (Choi et al, 2008; Huang et al, 2009).

Traditionally, the treatment efficacy on PWS is assessed on the basis of the change in skin color through the inspection of skin surface photographs at different time points during and after the treatment. Optical coherence tomography (OCT), which is widely used in current clinics (Zhou et al, 2012), is another potential modality that can be used to assess PWS and its response to treatment. OCT provides micrometer-level spatial resolution and millimeter-level imaging depth in real time (Baran et al, 2016). Variance analysis on a few subsequent OCT frames can be used to generate OCT angiography (OCT-A), providing three-dimensional (3D) blood perfusion assessment on top of morphological information at spatial resolution on the order of 10 μm (Baran et al, 2016; Deegan et al, 2018; Liu et al, 2021; Zhang et al, 2021).

Photo-mediated ultrasound therapy (PUT) is an antivascular technology based on the combination of synchronized ultrasound bursts and laser pulses. It utilizes the photoacoustic effect of pulsed laser light and spatiotemporally synchronizes laser pulses with ultrasound bursts to induce cavitation inside blood vessels. The laser energy and ultrasound amplitude used in PUT are significantly lower than those in traditional laser-only– and ultrasound-only–based therapeutic technologies. The mechanism of PUT based on the combination of low-energy laser and low-amplitude ultrasound ensures precise and selective treatment of blood vessels without damaging background tissues. In previous studies, PUTs have been applied to treat the retinal and choroidal microvessels in the eye (Qin et al, 2022, 2020a; Zhang et al, 2018). The feasibility of PUT to treat subcutaneous vessels has been tested using a rabbit ear model (Hu et al, 2017; Wang et al, 2020). These results demonstrated that blood perfusion can be significantly reduced after a single PUT treatment. In this study, we further investigated the feasibility of PUT for treatment of PWS in a chicken wattle model. Both the chicken comb model (Li et al, 2010; Orenstein et al, 1990) and the chicken wattle model (Rikihisa et al, 2018, 2017) have been extensively used in previous preclinical studies to understand the feasibilities of novel treatment modalities for improving PWS. Both models have a hypervascular dermis and morphology similar to human PWS and are thus considered clinically relevant (Rikihisa et al, 2018). During this study, by working on chicken wattles and utilizing OCT-A for assessment, we examined the treatment depth, efficacy, and safety of PUT for the treatment of PWS.

RESULTS

The study was carried out on 7 male Leghorn chickens. The first 2 chickens were used to titrate the PUT treatment parameters. Three chickens were used to perform treatments using either PUT, ultrasound only, or laser only with longitudinal OCT observation and histology evaluations. The remaining 2 chickens were used to perform PUT treatment and then killed on day 3 after treatment for additional immunohistochemistry evaluations.

During the titration of parameters for PUT treatment of chicken wattle, the initial set of treatment parameters was based on the previous work in a rabbit ear model (Wang et al, 2020). When tested in the chicken wattle model, we found that this initial set of treatment parameters did not lead to an efficient treatment response. Therefore, the negative peak pressure of the ultrasound bursts was gradually increased to 0.72 MPa, and the duty cycle was also increased from 0.2 to 2%, which led to a reduction of blood perfusion in the dermis observable on OCT-A. After that, the laser fluence was gradually increased to 707 mJ/cm^2 until PUT could completely stop the flow in all the blood vessels inside the treatment area, as indicated by OCT-A. Additional adjustments were made to the treatment duration (4 minutes) and the pulse repetition frequency (15 Hz). These final optimized treatment parameters, as shown in Table 1, were determined to minimize thermal damage and maximize blood vessel density reduction that could be achieved by PUT treatment of chicken wattle in vivo and were used later in the treatment of the remaining 5 chickens.

Figure 1a.1–a.3 shows the wattle skin photographs taken using the skin imaging camera immediately before treatment and on day 1 (immediately after) and day 14 after the treatment. It is a representative case in this study comparing 3 treatment spots on the same wattle: one with PUT, one with laser only, and one with ultrasound only. In these wattle skin photographs, a clearly visible change in color from red to white was observed on day 14 for the area treated by PUT. However, no such color change was observed in the areas treated by laser only or ultrasound only.

Besides using the skin imaging camera, the treatment outcome from PUT shown in Figure 1 was also evaluated by OCT-A. The red square shows the OCT scanning region on the wattle. Figure 1b.1–b.3 was obtained by overlapping the B-scan OCT-A images presenting the blood perfusion information over the B-scan OCT images presenting the tissue structural information. The B-scan was through the middle of the treatment spot marked by a dash blue line. As one can see in the OCT-A images, the blood perfusion was stopped the next day after PUT treatment (Figure 1b.2). This cessation in blood perfusion induced by PUT persisted until at least 14 days after the treatment (Figure 1b.3), which was the end of the observation period and when the chicken was killed for histopathology analysis. Figure 1c.1–c.3 is the maximum intensity projection images presenting the blood vessels within the depth range of 0 to 150 μm in the 3D OCT-A results. The scanned areas are marked by the red dash squares.

Table 1. Optimized Laser and Ultrasound Parameters for PUT of Blood Vessels in Chicken Wattle

Laser			Ultrasound				
Pulse Energy	Beam Diameter	Light Fluence	Peak Negative Pressure	Duty Cycle	Focal Width	Laser/Ultrasound Pulse Repetition Frequency	Treatment Duration
50 mJ	3 mm	707 mJ/cm^2	0.72 MPa	2 % (333 cycles)	6 mm	15 Hz	4 min

Abbreviation: PUT, photo-mediated ultrasound therapy.

The cessation of blood perfusion after the treatment can be observed as an area with reduced OCT-A intensity in the maximum-intensity projection images. This area with reduced OCT-A intensity has a diameter of around 3 mm, which is the same as the size of the treatment laser beam. Again, the cessation of blood perfusion was observed at least 14 days after the treatment, as shown in Figure 1c.3.

Assessment of PUT treatment outcome was performed by quantitatively analyzing the vessel density map generated from the 3D OCT-A images acquired before and at different time points after the treatment, as shown in Figure 2. In total, 7 treatments (n = 7) were carried out for each treatment group, including PUT, laser only, and ultrasound only, on a total of 3 chickens with the optimized PUT parameters. The maximum-intensity projection images of 3D OCT-A (0–150 µm depth in the dermis) of a PUT-treated region at different time points are shown in Figure 2b1–b5, and corresponding vessel density maps generated by the binarization of the maximum intensity projection images are shown in Figure 2c.1–c.5. This imaging processing procedure allowed quantitative and volumetric measurement of the change in vessel density in chicken wattle in vivo as a direct and fast assessment of the treatment efficacy. Figure 2d shows the normalized vessel density of all the regions treated with either PUT, laser only, or ultrasound only from day 0 (before treatment) to day 21 after treatment. Each data point shows the mean ± SD over 7 treatments in each group. For the PUT treatment group, the vessel density reduced by 73.23% on

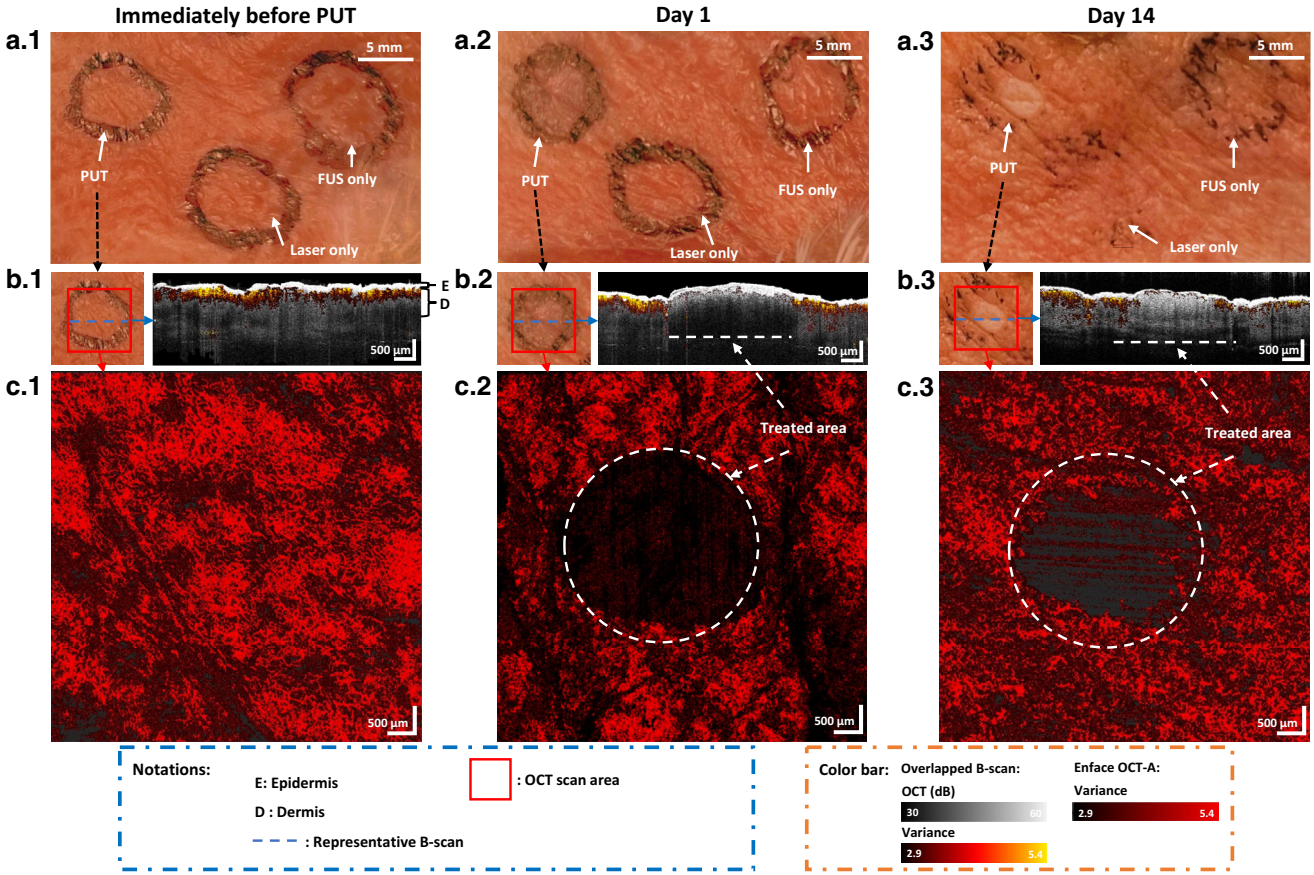

Figure 1. Representative treatment outcome from a chicken wattle treated with PUT. (**a.1**–**a.3**) Photographs of the chicken wattle taken before and at different time points after PUT treatment as well as laser-only and ultrasound-only treatment. (**b.1**–**b.3**) The B-scan OCT-A images overlapped on the B-scan OCT images acquired along the center of the treatment region shown in **a.1**–**a.3**. Images were acquired (**b.1**) immediately before and at different time points ([**b.2**] 1 day, [**b.3**] 14 days) after PUT treatment. (**c.1**–**c.3**) Maximum intensity projection images of 3D OCT-A of the areas marked in the red dash squares in **a.1**–**a.3**. The white circles mark the treated area. 3D, three-dimensional; FUS, focused ultrasound; OCT, optical coherence tomography; OCT-A, optical coherence tomography angiography; PUT, photo-mediated ultrasound therapy.

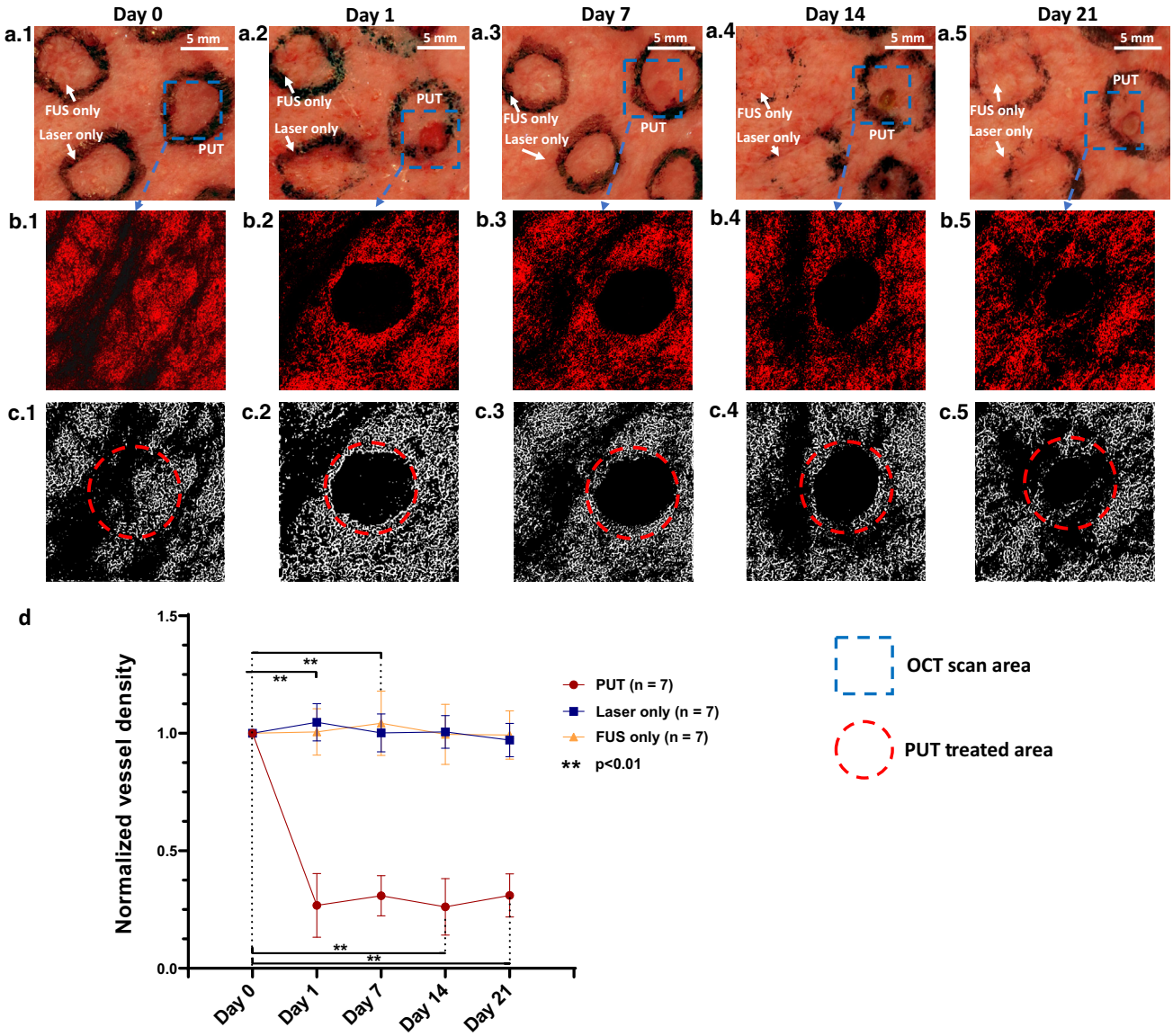

Figure 2. Quantitative assessment of vessel density changes in chicken wattles treated with either PUT, laser only, or ultrasound only. (**a.1**—**aa.5**) Photographs of a chicken wattle with 1 PUT-, 1 ultrasound-only—, and 1 laser-only—treated regions at different time points. (**b.1**—**b.5**) Maximum intensity projection images of 3D OCT-A (0—150 μm depth in the dermis) of the PUT-treated region at different time points. (**c.1**—**c.5**) Vessel density maps generated by binarization of the maximum intensity projection images in **b.1**—**b.5**. (**d**) Normalized vessel density of all the regions treated with either PUT (n = 7), laser only (n = 7), or ultrasound only (n = 7) from day 0 (before treatment) to day 21 after treatment, represented by mean ± SD. $^{**}P < 0.01$ for paired *t*-test between the measurement at each time point and the baseline measurement on day 0. (**a.1**—**c.1**) Day 0 (before the treatment), (**a.2**—**c.2**) Day 1 after the treatment, (**a.3**—**c.3**) Day 7 after the treatment, (**a.4**—**c.4**) Day 14 after the treatment, and (**a.5**—**c.5**) Day 21 after the treatment. 3D, three-dimensional; FUS, focused ultrasound; OCT, optical coherence tomography; OCT-A, optical coherence tomography angiography; PUT, photo-mediated ultrasound therapy.

day 1 (immediately after the treatment) and remained at a similar level until day 21. The quantified measurement of normalized vessel density on each time point after treatment was compared with the baseline measurement before treatment by a paired *t*-test, and statistically significant changes in vessel density were noticed in the PUT treatment group. For either ultrasound-only treatment group or the laser-only treatment group, no significant reduction in vessel density was observed.

Figures 3—5 show the H&E-stained histology results. Figure 3a is a section of wattle tissue harvested on day 21 after the PUT treatment, and the treatment area is marked with a red dash square. The blood vessel lumens completely disappeared at a depth of 0 to 400 μm from the wattle surface, as shown in Figure 3b. In addition, most of the capillary lumens are not visible in the 400—800 μm depth, except for 2 large blood vessels at the depth of 800 μm (Figure 3c), indicating a treatment depth of 700 μm for this case. The untreated region had abundant blood vessels, as illustrated in Figure 3d. In the untreated region, multiple vessel lumens ranging from 10 to 50 μm can be observed close to the epidermis as well as in the deep dermis up to the depth of 1000 μm. Figure 4a is a section of wattle tissue harvested on day 7 after the PUT treatment. This section, together with the magnified photographs in Figure 4b—d, confirms that the vessels in the wattle at a depth up to 800 μm from the wattle

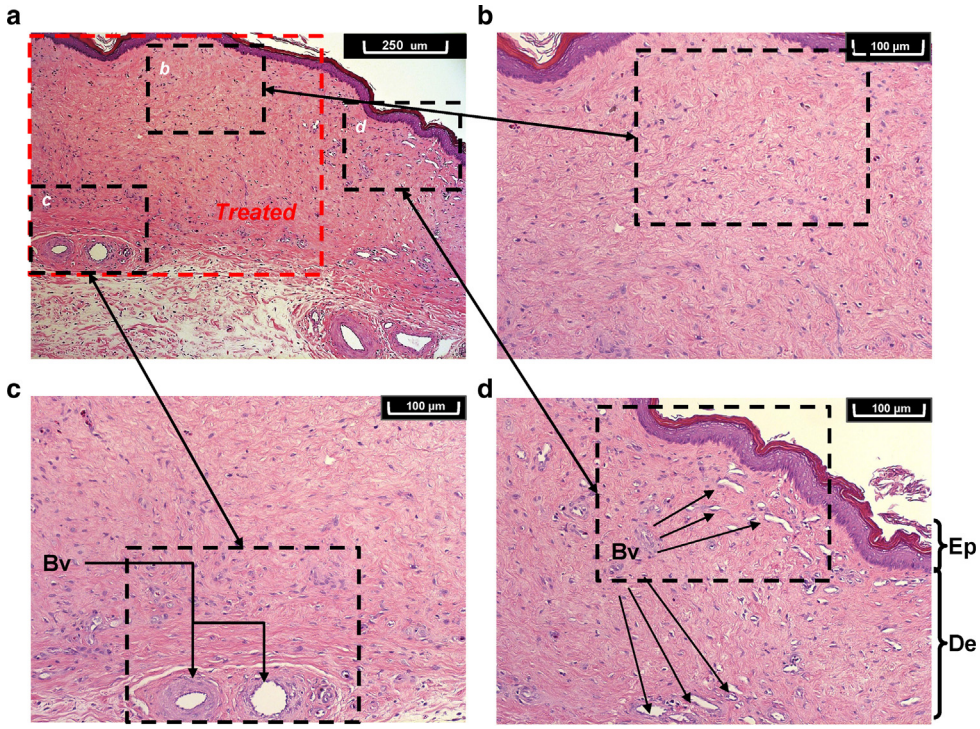

Figure 3. H&E-stained section of a wattle tissue harvested on day 21 after PUT treatment. (**a**) H&E-stained section of a wattle tissue harvested on day 21 after PUT treatment, ×10 magnification. The red dash square marks the treated area. (**b**) Enlarged view of a treated area close to the epidermis (0–400 μm depth), ×20 magnification. No blood vessels remain in the treated region. (**c**) Enlarged view of a treated area at 400–800 μm depth, ×20 magnification. Only large vessels remain. (**d**) Enlarged view of an untreated area where many blood vessels can be seen, ×20 magnification. Bv denotes blood vessels, Ep denotes epidermis, and De denotes dermis. PUT, photo-mediated ultrasound therapy.

surface were filled with red blood cells and degenerated endothelial cells after the treatment, whereas the overlying epidermis was left intact.

Figure 5 shows H&E-stained sections of wattle tissues treated with either PUT (Figure 5a–d), laser-only (Figure 5e), or ultrasound only (Figure 5f). The tissue sections showing the outcome from PUT were harvested on days 1, 7, 14, and 21 after the treatment. On days 1 and 7 after the PUT treatment, the vessels were occluded with red blood cells, whereas on days 14 and 21 after the PUT treatment, the vessel lumens in the treated regions disappeared. For comparison, in the sections treated with either ultrasound only or laser only, all blood vessels were completely intact on day 21 after the treatment.

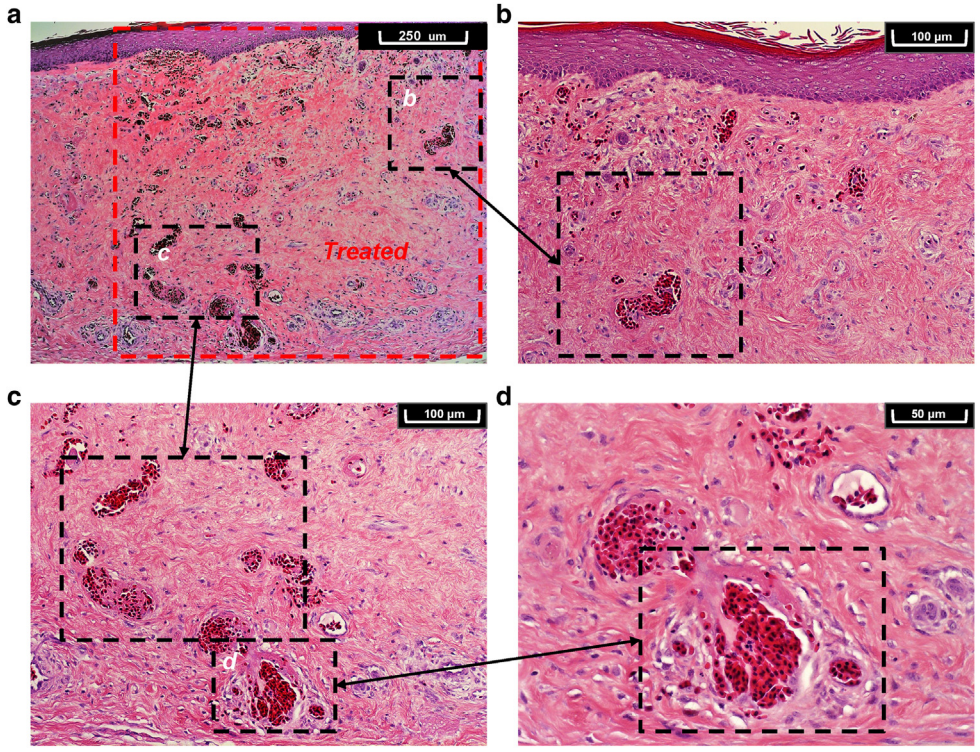

Figure 4. H&E-stained section of a wattle tissue harvested on day 7 after PUT treatment. (**a**) H&E-stained section of a wattle tissue harvested on day 7 after PUT treatment, ×10 magnification. The red dash square marks the treated area. (**b**) Enlarged view of a treated area close to the epidermis (0–400 μm depth), ×20 magnification. The vessel lumens are filled with erythrocytes, endothelial cells have degenerated, and the overlying epidermis is intact. (**c**) Enlarged view of a treated area at 400–800 μm depth, ×20 magnification. (**d**) Further enlarged view of a treated area at 800 μm depth, ×40 magnification. PUT, photo-mediated ultrasound therapy.

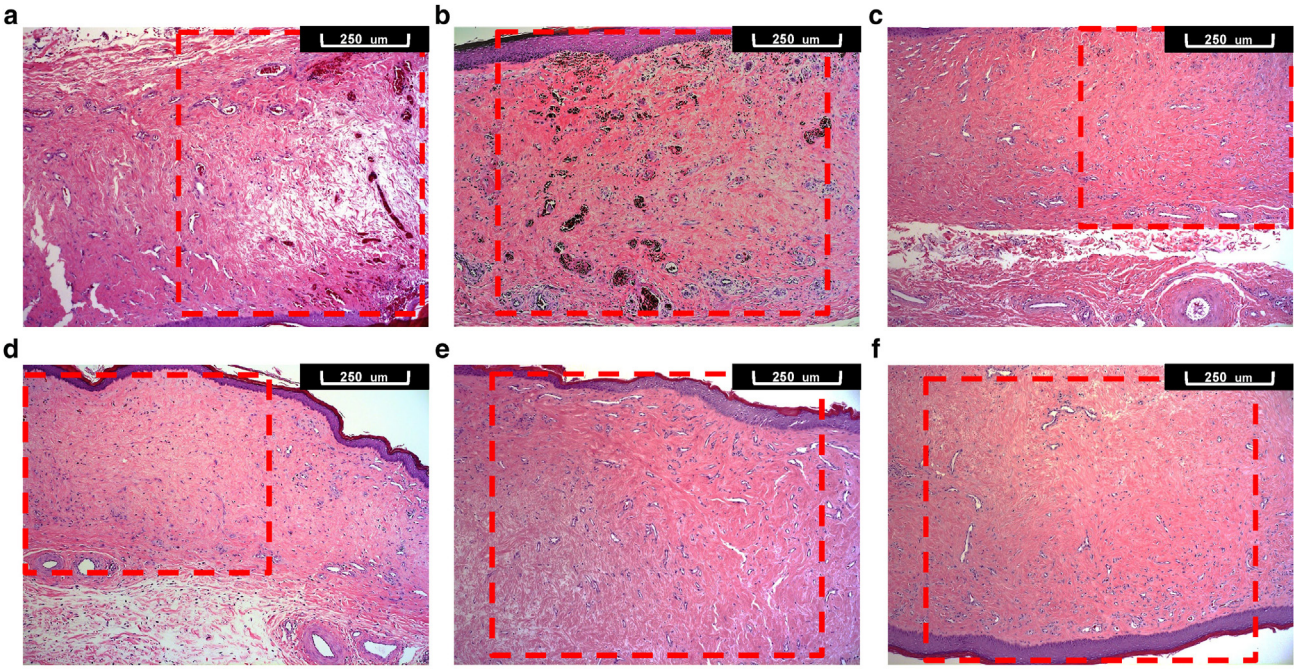

Figure 5. H&E-stained sections of wattle tissues. Shown are wattle tissues harvested on (**a**) day 1, (**b**) day 7, (**c**) day 14, and (**d**) day 21 after PUT treatment, ×10 magnification. (**e**) H&E-stained section of a wattle tissue harvested on day 21 after laser-only treatment, ×10 magnification. (**f**) H&E-stained section of a wattle tissue harvested on day 21 after ultrasound-only treatment, ×10 magnification. In each one, the treated area is marked by the red dash square. PUT, photomediated ultrasound therapy.

Additional immunohistochemistry evaluations of the treatment outcome were conducted on 2 chickens killed on day 3 after PUT treatment, and both treated and untreated wattle tissues were analyzed and compared. Tissue sections with 100-μm intervals were stained with CD31, H&E, caspase-3, and Masson's trichrome (MTC) so that tissues in the same vicinity could be subjected to different evaluations. As shown in Figure 6a and b, CD31-positive endothelial cells with clear vessel lumens can be seen in untreated tissue, whereas most endothelial cells in the treated area were found to be CD31 negative, indicating the desired vascular damage induced by PUT treatment. The H&E-stained histology results from the treated and untreated tissues in Figure 6c and d are comparable with those in Figure 4. The key findings in the treated area include clusters of red blood cells obstructing the blood vessel lumen and epidermis necrosis. Figure 7a and b show caspase-3 negative in both the untreated area and the dermis of the treated area. Some localized activations of caspase-3 were found in the epidermis of the treated area, which however were very minor. As shown by the MTC-stained histology results in Figure 7c and d, the collagen inside the treated area has structure and morphology similar to those in the untreated area, indicating no collateral collagen damage induced by the treatment.

DISCUSSION

During OCTA, the bulk tissue motion, often visible as horizontal lines, can sometimes negatively impact the image quality. However, the reduced image quality would not impact the final quantification results. This is because the image contrast between the treatment area and the surrounding area was huge, and differences are clearly visible even with all the motion artifacts (Figure 1c.3). Moreover, the binarization process shown in Figure 8 further eliminated the effect of motion artifacts from the final quantitative analyses.

The PUT treatment used in this study has a mechanism of action different from that of traditional PDL treatment. The widely used PDL therapy is based on the principle of selective heating of targets on the basis of the absorption of laser energy, also known as selective photothermolysis. In selective photothermolysis, the selected targets, such as capillaries and postcapillary venules in the case of PWS, absorb laser energy and are destroyed owing to heating without causing any significant damage to the surrounding tissues (Svaasand and Nelson, 2004).

In contrast, PUT, which uses laser pulses synchronized with ultrasound bursts, induces vascular bioeffects through the mechanical effects of cavitation. The nanosecond laser pulse irradiation of a vessel generates a photoacoustic wave, which results in high rarefaction pressure near the center of the vessel (Li et al, 2018). This photoacoustic wave, when superimposed on the peak negative pressure of an ultrasound wave, results in high rarefaction pressure and nucleates air cavities in the blood, also known as the photospallation effect (Hoffman and Telfair, 2000; Qin et al, 2020b). The nucleated air cavities or bubbles expand and compress inside the blood vessel owing to the simultaneous presence of an ultrasound wave. The PUT-induced cavitation interacts with blood vessels and generates stresses on the vessel wall (Singh and Yang, 2022; Singh et al, 2020). The stresses, mainly shear stress, impact the vascular endothelial cell functions and alter the release of vasoactive agents such as nitric oxide and prostacyclin, which ultimately results in vasculature degeneration (Karthikesh et al, 2022). On the basis of this unique

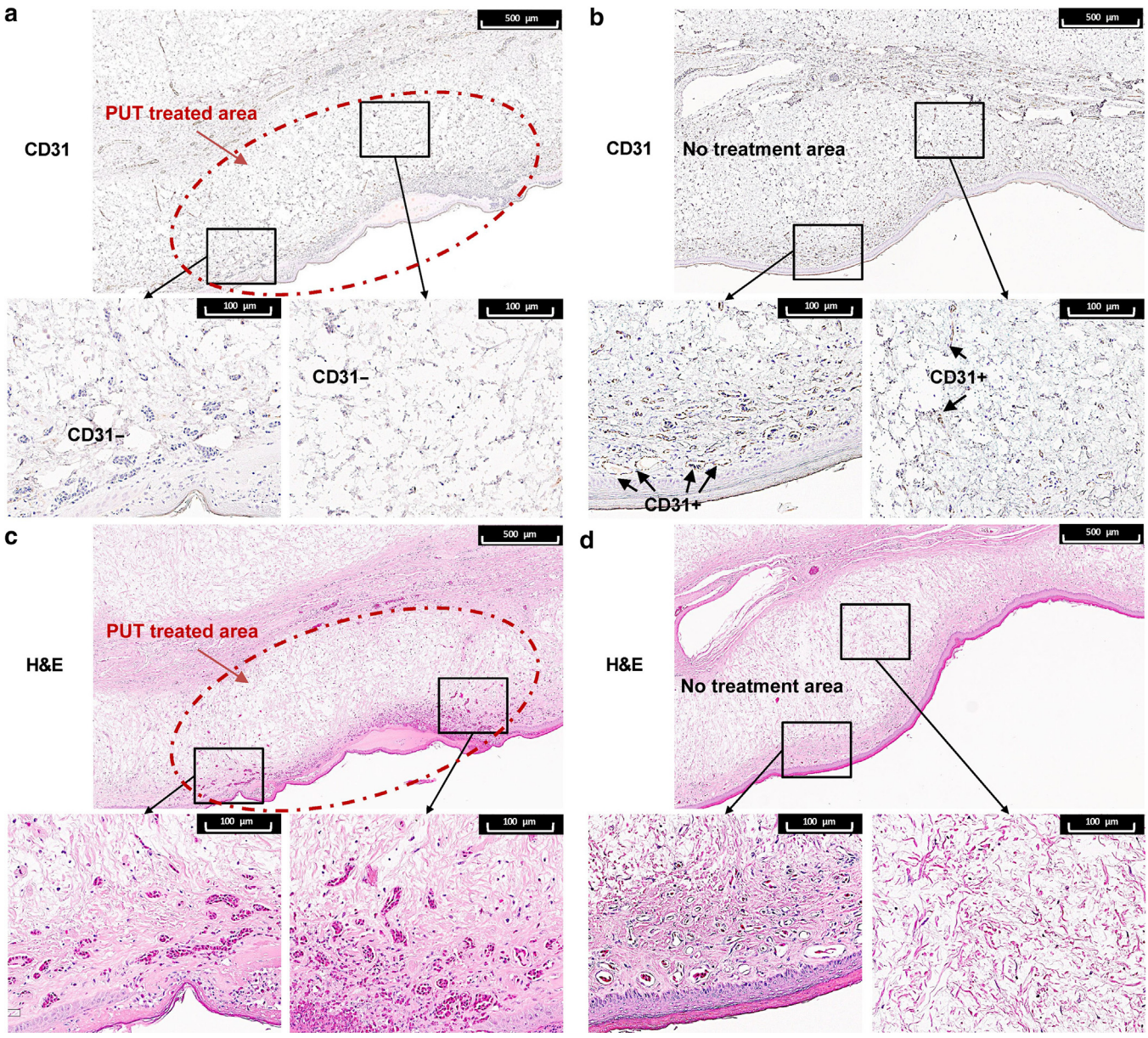

Figure 6. Safety evaluation on day 3 after PUT treatment. (**a**) CD31-stained section of a wattle tissue, including a treated area. (**b**) CD31-stained section of a wattle tissue that was untreated. (**c**) H&E-stained section of the same wattle tissue in **a**, including a treated area. (**d**) H&E-stained section of the same wattle tissue in **b** that was untreated. PUT, photo-mediated ultrasound therapy.

mechanism, we believe that there are 2 main potential advantages of PUT over the traditional PDL therapy for PWS, described in the following section.

Minimized thermal effect

Despite various epidermal cooling methods used during the treatment, such as contact cooling (Zenzie et al, 2000), air cooling (Raulin et al, 2000), and cryogen spray cooling (Nelson et al, 1995), unwanted thermal damage could not be completely avoided in pure laser-based PDL treatment owing to the thermal mechanism of action of PDL. The thermal side effects in PDL are due to the use of high laser fluence and millisecond domain laser pulse durations, which are necessary to induce sufficient heating in target vessels. In clinical studies on PWS, fluences of 3−300 J/cm^2 and pulse durations of 0.1−300 ms were used for 1064 nm laser treatment (van Drooge et al, 2013; Zhong et al, 2014), whereas in this study, the optimized laser fluence was 0.707 J/cm^2 for the 1064 nm laser with a pulse duration of 3−5 ns. During the treatment, the temperature on the wattle surface increased from an average of 23 to 35 °C during the 4-minute treatment. This increase in temperature during PUT was mainly due to the simultaneously applied ultrasound instead of the laser pulses. A temperature increase <20 °C from the baseline of 23 °C is considered safe because it is still below the denaturation threshold of collagen (Dewhirst et al, 2003; Pierce et al, 2004). In this study, immunohistochemistry and histology analyses involving CD31, H&E, caspase-3, and MTC stains provide evidence that PUT-induced therapeutic effect is confined and specific to blood vessels only, whereas unwanted collateral damage in other skin tissues such as collagen are avoided.

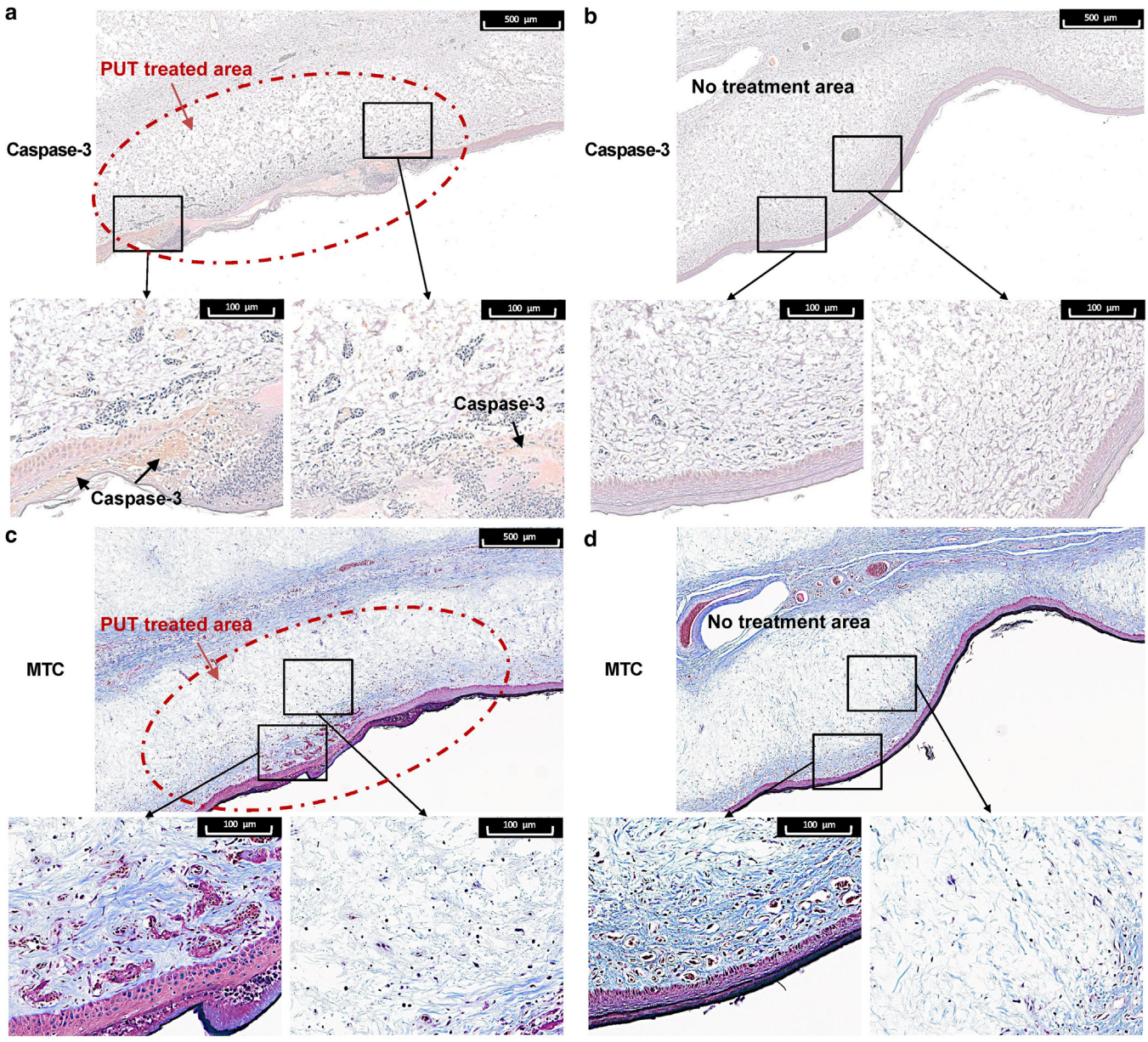

Figure 7. Safety evaluation on day 3 after PUT treatment. (**a**) Caspase-3–stained section of a wattle tissue, including a treated area. (**b**) Caspase-3–stained section of a wattle tissue that was untreated. (**c**) MTC-stained section of the same wattle tissue in **a**, including a treated area. (**d**) MTC-stained section of the same wattle tissue in **b** that was untreated. MTC, Masson's trichrome; PUT, photo-mediated ultrasound therapy.

Treatment depth

The OCT-A images in this study showed that almost all the blood vessels within the depth range of 0 to 150 μm in the dermis of the chicken wattle were removed by PUT. However, this 150-μm depth is not the limitation of the PUT treatment depth but instead the OCT-A imaging depth, which is limited by the extremely dense vasculature in chicken wattle tissue. The histology and immunohistochemistry results further validated that the treatment depth of PUT could reach up to 0.8 mm. Previous clinical studies have reported treatment depths of up to 2 mm when using 1064 nm laser (Kelly et al, 2005). In this study, the observed treatment depth in PUT was limited by the structure of the chicken wattle as discussed below. Technically, it is possible to achieve a much greater treatment depth in PUT using 1064 nm light, which has the highest penetration depth and lowest melanin absorption among all the laser wavelengths currently used for treatment of PWS. The 1064 nm is not widely used in the treatment of PWS owing to the increased risk of thermal side effects, including scarring, when working with high laser fluences. In contrast, the 1064 nm laser can be safely used in PUT without causing collateral thermal damage in background skin tissues. This is because PUT treatment of blood vessels is not based on the laser-based heating of vessels but instead based on the photoacoustic effect induced by nanosecond laser pulses. When working with spatiotemporally synchronized ultrasound bursts, PUT can eliminate blood vessels when utilizing much lower light energy levels. Apart from the laser wavelength, the treatment depth of PUT also depends on spatial synchronization between ultrasound and

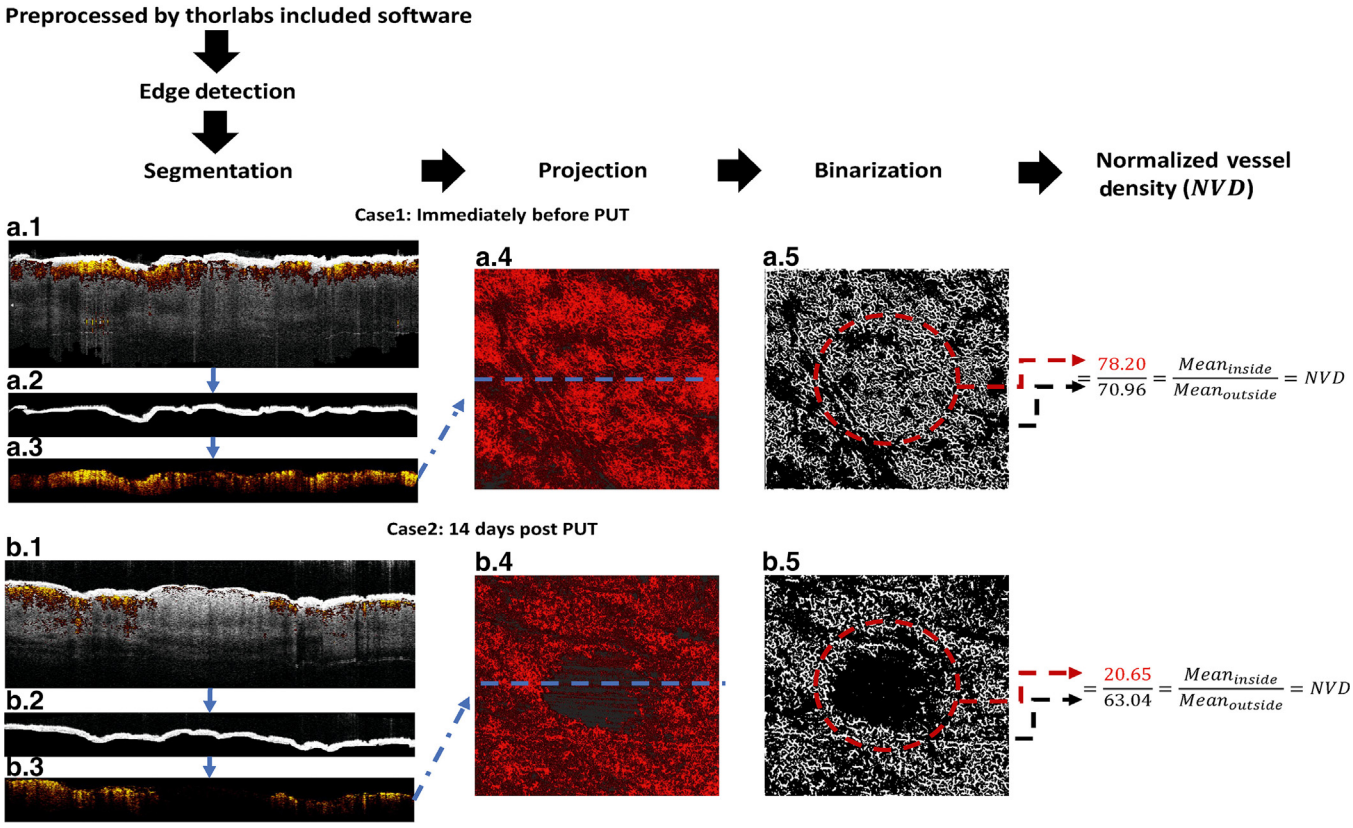

Figure 8. Data processing schematic. Two cases are presented for the chicken wattle tissue (**a**) immediately before PUT treatment and (**b**) 14 days after PUT treatment. (**a.1, b.1**) The B-scan OCT-A images overlapped on the B-scan OCT images along the center of treatment regions marked in **a.4** and **b.4**. (**a.2, b.2**) The surface of the skin and the area of the epidermis segmented from the B-scan OCT images. (**a.3, b.3**) The segmented layer with 0–150 μm depth in the dermis for analyzing the OCT-A signals. (**a.4, b.4**) En face projections of the OCT-A signals in the segmented layer. (**a.5, b.5**) Binarization results of the en face projections of the OCT-A signals in the segmented layer. OCT, optical coherence tomography; OCT-A, optical coherence tomography angiography; PUT, photomediated ultrasound therapy.

laser. The treatment threshold in PUT depends on the combination of ultrasound bursts and laser pulses. Ultrasound can penetrate deeper into the skin without much scattering, whereas laser energy decreases much faster with the depth of penetration owing to the strong scattering and absorption of light in skin tissues. With PUT, the low laser energy at greater dermal depths can be compensated for by focusing the ultrasound energy at specific locations. Hence, a combination of high ultrasound energy and low laser energy at deep dermis and a combination of low ultrasound energy and high laser energy at superficial dermis can both produce cavitation of PWS vessels. This potentially makes PUT a flexible and effective treatment for a wide variety of these heterogeneous vascular lesions.

In conclusion, this study demonstrated that PUT, which uses spatiotemporally synchronized laser pulses and ultrasound bursts, was effective in eliminating blood vessels in a clinically relevant chicken wattle model of PWS in vivo. The laser fluence used in this study was 10–100 times lower than that used in traditional PDL therapy. Using a laser fluence of only 0.707 J/cm2 at a wavelength of 1064 nm combined with ultrasound bursts, a decrease in blood vessel density in the chicken wattle by 73.23% with a treatment depth of up to 1 mm from the skin surface was achieved after a single PUT treatment without causing collateral thermal damage in surrounding tissues. Further clinical studies are required to assess this promising antivascular technology in the treatment of PWS.

MATERIALS AND METHODS

Experimental setup

A detailed schematic of the PUT system is shown in Figure 9. The PUT system was a combination of a focused ultrasound (FUS) system and a pulsed laser system. The laser source was a Q-switched Nd-YAG laser (Minilite II, Continuum Electro-Optics), which emitted 1064-nm wavelength pulses with 5–7 ns pulse width. The laser repetition rate and pulse energy in the range of 0–15 Hz and 0–50 mJ, respectively, were controlled through a delay generator (DG535, Stanford Research Systems). The ultrasound bursts were produced by a FUS transducer with 0.25 MHz central frequency (H-117, Sonic Concepts). The transducer had a radius of curvature of 63.2 mm with a focal depth and focal width of 6 and 40 mm, respectively. The sine wave burst for FUS was produced by a function generator (DG345, Stanford Research Systems) and was amplified by a power amplifier (2100L, Electronics & Innovation) before being passed to the FUS transducer through an impedance-matching circuit. A delay generator was used to trigger both the FUS system and the laser system to temporally synchronize the ultrasound bursts and laser pulses over the treatment area.

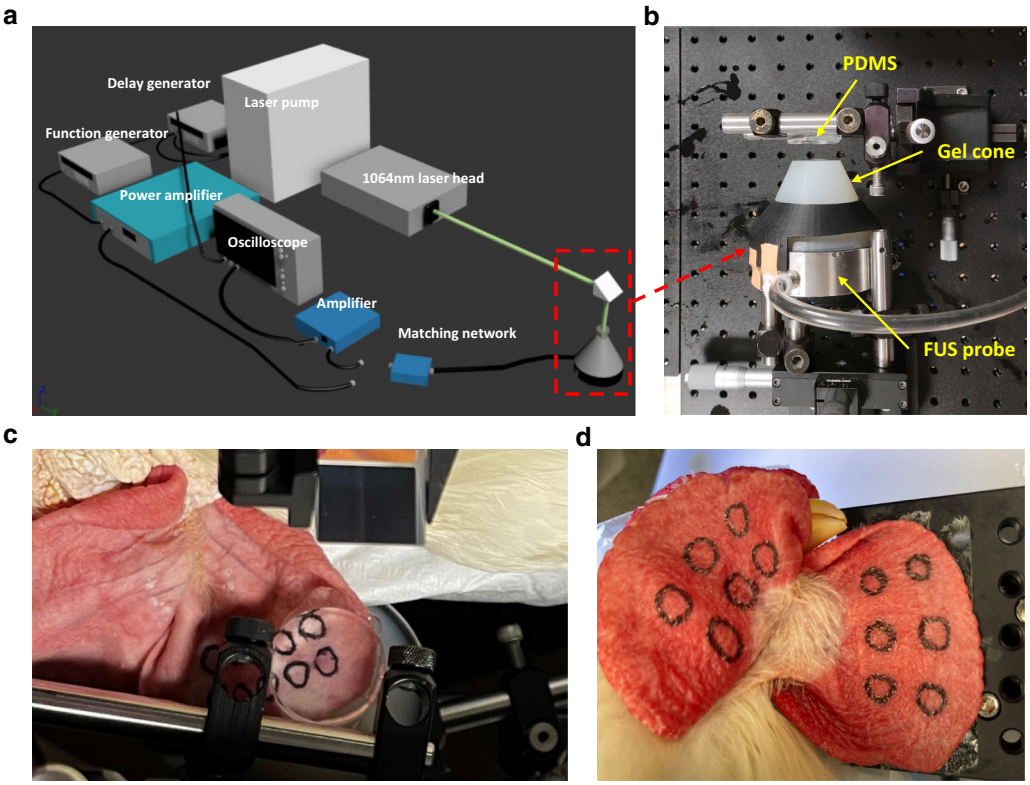

Figure 9. System schematic and experiment setup for PUT treatment of chicken wattle. (**a**) Detailed schematic of the integrated ultrasound and laser system for PUT treatment of chicken wattle. (**b**) Photo of the experimental setup showing positions of an agar-gelatin gel cone and a PDMS pad. (**c**) Photo of a chicken wattle positioned between the PDMS and the gel cone during the treatment. (**d**) Pretreatment picture of a chicken wattle, with marked circles indicating the spots to be treated. FUS, focused ultrasound; PDMS, polydimethylsiloxane; PUT, photo-mediated ultrasound therapy.

Treatment procedure

Before the treatment, the roosters were anesthetized by injecting a mixture of ketamine (15 mg/kg) and xylazine (0.6 mg/kg) intramuscularly. After anesthesia, the chicken wattle inner surface was marked with black circular marks at 6–8 different spots to indicate the treatment regions, as shown in Figure 9d. For the treatment, the wattle was placed between an agar gelatin cone and a polydimethylsiloxane (PDMS) pad such that the ultrasound energy could be delivered to the wattle through the gel cone and the laser energy could be delivered to the wattle through the PDMS pad (Figure 9b). The purpose of PDMS was to reduce ultrasound energy deposition at the wattle surface. The ultrasound coupling gel was applied at the cone–wattle and the wattle–PDMS interfaces to ensure efficient ultrasound delivery to the wattle. Moreover, a slight pressure was applied through the PDMS pad to restrict the wattle movement during the treatment. When positioning the wattle with respect to the transducer, the laser pulse was emitted on the target area to generate a photoacoustic signal, which was captured by the transducer, received by the amplifier, and shown on the oscilloscope. Then, the position of the transducer was adjusted by a 3D stage until the photoacoustic signal reached its maximum amplitude to ensure that the ultrasound beam and the laser beam irradiated over the same region on the wattle. The PUT treatment at each spot was performed for <5 minutes, and the total treatment time for each chicken wattle was <40 minutes. During the entire treatment, a noncontact thermal temperature sensing device (NF-521, Noyafa) was used to monitor the temperature on the wattle surface in real time.

Data collection, processing, and statistical analyses

To evaluate the treatment outcome, the treatment areas on the chicken wattle were imaged by a Canfield skin imaging camera (Canon EOS camera-based, Canfield Scientific) and a laboratory, nonclinical spectral domain OCT system (TEL 321 Telesto, Thorlabs). The images were taken at different time points, which were before the treatment (control) and on day 1 (short term), day 7, day 14, and day 21 (long-term) after the treatment. Photos taken by the skin imaging camera were used to assess the changes in skin color after white balance was matched by the histomatch algorithms using MATLAB. Quantitative analyses of the changes in vessel density after treatment were conducted using the imaging results from the spectral domain OCT system, which has an image depth of 2.6 mm in water. Both OCT and OCT-A data were collected during the spectral domain OCT imaging using the software provided by Thorlabs. OCT-A data were generated using a speckle variance analysis over 3 repeated B-scans per position. To quantitatively analyze the vascular density changes, the process detailed in Figure 8 was conducted. First, skin surface detection was done using OCT volume data. After acquiring a single layer at the top surface, the OCT-A data were depth encoded. Then, the OCT-A signals in the dermis between 0 and 150 μm were extracted, and the maximum intensity projection was used to create a two-dimensional map. To create a vascular density map, a binarization of this two-dimensional perfusion map was performed. On the binarized two-dimensional map, mean vessel densities within and outside the treatment region were measured to establish normalized vessel densities. Statistical analyses were performed using GraphPad Prism 9.0.0 (GraphPad Software) and presented as mean ± SD in

Figure 2d. *P*-values were derived from paired *t*-tests comparing normalized vessel densities at different time points, and $P < .05$ was determined as statistically significant.

Histology and immunohistochemistry analysis

Chicken wattle samples were collected after the chickens were killed at different time points (days 1, 3, 7, 14, and 21) after the treatment. The tissues for histology and immunohistochemistry were stained with H&E, CD31 antibodies, caspase-3 antibodies, and MTC, which were performed by the In Vivo Animal Core in the Unit for Laboratory Animal Medicine at the University of Michigan (Ann Arbor, MI).

Paraffin processing and sectioning

Briefly, formalin-fixed tissues were processed through graded alcohols and cleared with xylene followed by infiltration with molten paraffin using an automated VIP5 or VIP6 tissue processor (Tissue-Tek, Sakura-Americas). After paraffin embedding using a Histostar Embedding Station (Thermo Fisher Scientific), tissues were then sectioned on an M 355S rotary microtome (Thermo Fisher Scientific) at 4-μm thickness and mounted on glass slides.

H&E staining

After deparaffinization and hydration with xylene and graded alcohols, formalin-fixed, paraffin-embedded slides were stained on an automated histostainer (Autostainer XL, Leica Biosystems) with Harris hematoxylin (Thermo Fisher Scientific, catalog number 842); differentiated with Clarifier (Thermo Fisher Scientific, catalog number 7401); blued with bluing reagent (Thermo Fisher Scientific, catalog number 7301); stained with eosin Y, alcoholic (Thermo Fisher Scientific, catalog number 832), then dehydrated and cleared through graded alcohols and xylene, and coverslipped with Micromount (Leica Biosystems, catalog number 3801731) using a Leica CV5030 automatic coverslipper.

MTC staining

All staining reagents were obtained commercially from Rowley Biochemical (Danvers, MA) unless otherwise noted. Briefly, after deparaffinization and hydration with xylene and graded alcohols, formalin-fixed, paraffin-embedded slides were mordanted in Bouin's Fixative (F-367-1) for 1 hour at 56 °C. After a thorough rinse in water, slides were placed in Biebrich Scarlet-Acid Fuchsin (F-367-3) for 15 minutes at room temperature, phosphotungstic-phosphomolybdic acid (F-367-4) for 15 minutes at room temperature, and aniline blue stain (F-367-5) for 8 minutes at room temperature. Slides were then dehydrated and cleared through graded alcohols and xylene and coverslipped with Micromount (Leica Biosystems, catalog number 3801731) using a Leica CV5030 automatic coverslipper.

Immunohistochemical staining

After deparaffinization and hydration with xylene and graded alcohols, formalin-fixed, paraffin-embedded slides were subjected to heat-induced epitope retrieval in Diva Decloaking Buffer, pH 6.2 (Biocare Medical), in a pressure cooker (Biocare Medical). Immunohistochemical staining was performed on an automated IntelliPATH FLX immunohistochemical stainer (Biocare Medical) and included blocking for endogenous peroxidase and nonspecific binding, primary antibody incubation, detection using a horseradish peroxidase biotin-free polymer-based system, disclosure with diaminobenzidine chromogen, and nuclear counterstaining with hematoxylin.

Specific to cleaved caspase-3 (Cell Signaling Technology, catalog number 9664), the rabbit monoclonal primary antibody was diluted to 1:500 in DaVinci Diluent (Biocare Medical, catalog number PD900) and incubated for 30 minutes followed by detection using Rabbit on Rodent HRP-Polymer (Biocare Medical, catalog number RMR622) for 30 minutes. Negative control samples consisted of naïve serum (Universal Negative, Biocare Medical) applied in place of the primary antibody, under the same conditions.

Specific to CD31 (Dianova, number SZ31), rat monoclonal primary antibody was diluted to 1:50 in DaVinci Diluent (Biocare Medical, catalog number PD900) and incubated for 60 minutes, followed by detection using a Rat-on-Mouse HRP-Polymer (Biocare Medical, catalog number RT517) 2-step probe-polymer incubation for 10 and 30 minutes, respectively. The diaminobenzidine was enhanced with diaminobenzidine Sparkle (Biocare Medical, catalog number DS830). Negative control samples consisted of naïve rat sera (NC915, Innovex Biosciences) applied in place of the primary antibody, under the same conditions.

Ethics statement

All the animal handling procedures were carried out in compliance with the protocol approved by the Institutional Animal Care and Use Committee at the University of Michigan (protocol number PRO00009939; principal investigator: XW).

Data availability statement

No large datasets were generated or analyzed during this study. Minimal datasets necessary to interpret and/or replicate data in this paper are available upon request to the corresponding author.

ORCIDs

Mingyang Wang: http://orcid.org/0000-0002-4076-1643
Rohit Singh: http://orcid.org/0000-0002-8415-6728
Wei Zhang: http://orcid.org/0000-0002-2539-8321
Jeffrey S. Orringer: http://orcid.org/0000-0001-5498-308X
Yannis M. Paulus: http://orcid.org/0000-0002-0615-628X
Xinmai Yang: http://orcid.org/0000-0001-8120-6593
Xueding Wang: http://orcid.org/0000-0002-2974-6258

ACKNOWLEDGMENTS

This work was funded in part by grants from the National Institutes of Health, United States (R41EB030875 to XW and XY), the National Eye Institute (R01EY029489 to XY, 1K08EY027458 and 1R41EY031219 to YMP), Alcon Research Institute Young Investigator Grant (to YMP), Fight for Sight- International Retinal Research Foundation (FFSGIA16002 to YMP), the Helmut F. Stern Career Development Professorship in Ophthalmology and Visual Sciences (to YMP), the Alliance for Vision Research (to YMP), unrestricted departmental support from Research to Prevent Blindness (to YMP), generous support of the Helmut F. Stern Career Development Professorship in Ophthalmology and Visual Sciences (to YMP), and the University of Michigan Department of Ophthalmology and Visual Sciences. This research utilized the Core Center for Vision Research funded by the National Eye Institute (P30 EY007003). The authors acknowledge the histology services and interpretation provided by the In Vivo Animal Core in the Unit for Laboratory Animal Medicine at the University of Michigan.

AUTHOR CONTRIBUTIONS

Conceptualization: MW, RS, YMP, XY, XW; Data Curation: MW, RS, WZ; Supervision: YMP, XY, XW; Visualization: MW; Writing - Original Draft Preparation: MW, RS; Writing - Review and Editing: JSO, YMP, XY, XW

CONFLICT OF INTEREST

YMP, XY, and XW serve as coinventors on a United States patent jointly owned by the University of Kansas and the University of Michigan on photo-mediated ultrasound therapy technology and have equity in PhotoSonoX LLC.

REFERENCES

Asahina A, Watanabe T, Kishi A, Hattori N, Shirai A, Kagami S, et al. Evaluation of the treatment of port-wine stains with the 595-nm long pulsed dye laser: a large prospective study in adult Japanese patients. J Am Acad Dermatol 2006;54:487–93.

Baran U, Choi WJ, Wang RK. Potential use of OCT-based microangiography in clinical dermatology. Skin Res Technol 2016;22:238–46.

Chen JK, Ghasri P, Aguilar G, van Drooge AM, Wolkerstorfer A, Kelly KM, et al. An overview of clinical and experimental treatment modalities for port wine stains. J Am Acad Dermatol 2012;67:289–304.

Choi B, Jia W, Channual J, Kelly KM, Lotfi J. The importance of long-term monitoring to evaluate the microvascular response to light-based therapies. J Invest Dermatol 2008;128:485–8.

Deegan AJ, Talebi-Liasi F, Song S, Li Y, Xu J, Men S, et al. Optical coherence tomography angiography of normal skin and inflammatory dermatologic conditions. Lasers Surg Med 2018;50:183–93.

Dewhirst MW, Viglianti BL, Lora-Michiels M, Hoopes PJ, Hanson M. Thermal dose requirement for tissue effect: experimental and clinical findings. Proc SPIE Int Soc Opt Eng 2003;4954:37.

Eivazi B, Roessler M, Pfützner W, Teymoortash A, Werner JA, Happle R. Port-wine stains are more than skin-deep! Expanding the spectrum of extracutaneous manifestations of nevi flammei of the head and neck. Eur J Dermatol 2012;22:246–51.

Fu Z, Huang J, Xiang Y, Huang J, Tang Z, Chen J, et al. Characterization of laser-resistant port wine stain blood vessels using in vivo reflectance confocal microscopy. Lasers Surg Med 2019;51:841–9.

Geronemus RG, Quintana AT, Lou WW, Kauvar AN. High-fluence modified pulsed dye laser photocoagulation with dynamic cooling of port-wine stains in infancy. Arch Dermatol 2000;136:942–3.

Hoffman HJ, Telfair WB. Photospallation: a new theory and mechanism for mid-infrared corneal ablations. J Refract Surg 2000;16:90–4.

Hu Z, Zhang H, Mordovanakis A, Paulus YM, Liu Q, Wang X, et al. High-precision, non-invasive anti-microvascular approach via concurrent ultrasound and laser irradiation. Sci Rep 2017;7:40243.

Huang YC, Tran N, Shumaker PR, Kelly K, Ross EV, Nelson JS, et al. Blood flow dynamics after laser therapy of port wine stain birthmarks. Lasers Surg Med 2009;41:563–71.

Izikson L, Anderson RR. Treatment endpoints for resistant port wine stains with a 755 nm laser. J Cosmet Laser Ther 2009;11:52–5.

Izikson L, Nelson JS, Anderson RR. Treatment of hypertrophic and resistant port wine stains with a 755 nm laser: a case series of 20 patients. Lasers Surg Med 2009;41:427–32.

Jacobs AH, Walton RG. The incidence of birthmarks in the neonate. Pediatrics 1976;58:218–22.

Karthikesh MS, Wu S, Singh R, Paulus Y, Wang X, Yang X. Effect of photo-mediated ultrasound therapy on nitric oxide and prostacyclin from endothelial cells. Appl Sci (Basel) 2022;12:2617.

Kelly KM, Choi B, McFarlane S, Motosue A, Jung B, Khan MH, et al. Description and analysis of treatments for port-wine stain birthmarks. Arch Facial Plast Surg 2005;7:287–94.

Kono T, Sakurai H, Takeuchi M, Yamaki T, Soejima K, Groff WF, et al. Treatment of resistant port-wine stains with a variable-pulse pulsed dye laser. Dermatol Surg 2007;33:951–6.

Li S, Qin Y, Wang X, Yang X. Bubble growth in cylindrically-shaped optical absorbers during photo-mediated ultrasound therapy. Phys Med Biol 2018;63:125017.

Li W, Yamada I, Masumoto K, Ueda Y, Hashimoto K. Photodynamic therapy with intradermal administration of 5-aminolevulinic acid for port-wine stains. J Dermatolog Treat 2010;21:232–9.

Liu Y, Chen D, Xu J, Tan Y, Wang Y, Zhao H, et al. Quantitative assessment of vascular features in port wine stains through optical coherence tomography angiography. Photodiagnosis Photodyn Ther 2021;36:102607.

Lu YG, Wu JJ, Yang YD, Yang HZ, He Y. Photodynamic therapy of port-wine stains. J Dermatolog Treat 2010;21:240–4.

Morelli JG, Tan OT, Garden J, Margolis R, Seki Y, Boll J, et al. Tunable dye laser (577 nm) treatment of port wine stains. Lasers Surg Med 1986;6:94–9.

Nelson JS, Milner TE, Anvari B, Tanenbaum BS, Kimel S, Svaasand LO, et al. Dynamic epidermal cooling during pulsed laser treatment of port-wine stain. A new methodology with preliminary clinical evaluation. Arch Dermatol 1995;131:695–700.

Orenstein A, Nelson JS, Liaw LH, Kaplan R, Kimel S, Berns MW. Photochemotherapy of hypervascular dermal lesions: a possible alternative to photothermal therapy? Lasers Surg Med 1990;10:334–43.

Pierce MC, Sheridan RL, Hyle Park B, Cense B, de Boer JF. Collagen denaturation can be quantified in burned human skin using polarization-sensitive optical coherence tomography. Burns 2004;30:511–7.

Qin Y, Yu Y, Fu J, Wang M, Yang X, Wang X, et al. Photo-mediated ultrasound therapy for the treatment of retinal neovascularization in rabbit eyes. Lasers Surg Med 2022;54:747–57.

Qin Y, Yu Y, Fu J, Xie X, Wang T, Woodward MA, et al. Photo-mediated ultrasound therapy for the treatment of corneal neovascularization in rabbit eyes. Transl Vis Sci Technol 2020a;9:16.

Qin Y, Yu Y, Xie X, Zhang W, Fu J, Paulus YM, et al. The effect of laser and ultrasound synchronization in photo-mediated ultrasound therapy. IEEE Trans Biomed Eng 2020b;67:3363–70.

Raulin C, Greve B, Hammes S. Cold air in laser therapy: first experiences with a new cooling system. Lasers Surg Med 2000;27:404–10.

Rikihisa N, Tominaga M, Watanabe S, Mitsukawa N, Saito Y, Sakai H. Intravenous injection of artificial red cells and subsequent dye laser irradiation causes deep vessel impairment in an animal model of port-wine stain. Lasers Med Sci 2018;33:1287–93.

Rikihisa N, Watanabe S, Satoh K, Saito Y, Sakai H. Photosensitizer effects of artificial red cells on dye laser irradiation in an animal model assuming port-wine stain treatment. Plast Reconstr Surg 2017;139:707e–16e.

Savas JA, Ledon JA, Franca K, Chacon A, Nouri K. Pulsed dye laser-resistant port-wine stains: mechanisms of resistance and implications for treatment. Br J Dermatol 2013;168:941–53.

Singh R, Wang X, Yang X. Cavitation induced shear and circumferential stresses on blood vessel walls during photo-mediated ultrasound therapy. AIP Adv 2020;10:125227.

Singh R, Yang X. A 3D finite element model to study the cavitation induced stresses on blood-vessel wall during the ultrasound-only phase of photo-mediated ultrasound therapy. AIP Adv 2022;12:045020.

Svaasand LO, Nelson JS. On the physics of laser-induced selective photothermolysis of hair follicles: influence of wavelength, pulse duration, and epidermal cooling. J Biomed Opt 2004;9:353–61.

Tan OT, Murray S, Kurban AK. Action spectrum of vascular specific injury using pulsed irradiation. J Invest Dermatol 1989;92:868–71.

van Drooge AM, Bosveld B, van der Veen JP, de Rie MA, Wolkerstorfer A. Long-pulsed 1064 nm Nd:YAG laser improves hypertrophic port-wine stains. J Eur Acad Dermatol Venereol 2013;27:1381–6.

Wang M, Qin Y, Wang T, Orringer JS, Paulus YM, Yang X, et al. Removing subcutaneous microvessels using photo-mediated ultrasound therapy. Lasers Surg Med 2020;52:984–92.

Wanitphakdeedecha R, Ng JNC, Yan C, Manuskiatti W, Sudhipongpracha T, Jantarakolica T. Quality of life and psychological effects of port-wine stain: a review of literature. Clin Cosmet Investig Dermatol 2021;14:681–90.

Woo SH, Ahn HH, Kim SN, Kye YC. Treatment of vascular skin lesions with the variable-pulse 595 nm pulsed dye laser. Dermatol Surg 2006;32:41–8.

Yuan KH, Li Q, Yu WL, Huang Z. Photodynamic therapy in treatment of port wine stain birthmarks–recent progress. Photodiagnosis Photodyn Ther 2009;6:189–94.

Yuan KH, Li Q, Yu WL, Zeng D, Zhang C, Huang Z. Comparison of photodynamic therapy and pulsed dye laser in patients with port wine stain birthmarks: a retrospective analysis. Photodiagnosis Photodyn Ther 2008;5:50–7.

Zenzie HH, Altshuler GB, Smirnov MZ, Anderson RR. Evaluation of cooling methods for laser dermatology. Lasers Surg Med 2000;26:130–44.

Zhang H, Xie X, Li J, Qin Y, Zhang W, Cheng Q, et al. Removal of choroidal vasculature using concurrently applied ultrasound bursts and nanosecond laser pulses. Sci Rep 2018;8:12848.

Zhang Y, Li H, Cao T, Chen R, Qiu H, Gu Y, et al. Automatic 3D adaptive vessel segmentation based on linear relationship between intensity and complex-decorrelation in optical coherence tomography angiography. Quant Imaging Med Surg 2021;11:895–906.

Zhong SX, Liu YY, Yao L, Song Y, Zhou JF, Zu JJ, et al. Clinical analysis of port-wine stain in 130 Chinese patients treated by long-pulsed 1064-nm Nd:YAG laser. J Cosmet Laser Ther 2014;16:279–83.

Zhou Y, Yin D, Xue P, Huang N, Qiu H, Wang Y, et al. Imaging of skin microvessels with optical coherence tomography: potential uses in port wine stains. Exp Ther Med 2012;4:1017–21.